

OPTIMIZED DESIGN, FABRICATION AND CHARACTERIZATION OF PZT UNIMORPH MICROACTUATORS FOR DEFORMABLE MIRRORS

Yoshikazu Hishinuma and Eui-Hyeok Yang

Jet Propulsion Laboratory

4800 Oak Grove Drive, Pasadena, CA 91109-8099

Yoshikazu.Hishinuma@jpl.nasa.gov ph: +1-818-393-9063 fx: +1-818-393-6047

Jian-Gong Cheng and Susan Trolier-McKinstry

Pennsylvania State University

151 Materials Research Laboratory

The Pennsylvania State University

University Park, PA 16802

ABSTRACT

This paper describes an optimization of PZT unimorph membrane microactuators in view of their application to deformable mirrors (DMs). PZT unimorph actuators of various electrode designs, silicon membrane thickness, and membrane sizes were fabricated and characterized. A mathematical model was developed to further assist the optimization of membrane thickness and electrode sizes, and excellent agreement with experiment was obtained. For a 2.5mm diameter actuator with 2 μ m thick PZT and 15 μ m thick silicon membrane, the measured vertical stroke was 5.4 μ m at 50V. The measured resonant frequency of the unimorph actuator was 47kHz, far exceeding the bandwidth requirement of most DMs (~1kHz).

INTRODUCTION

A key optical component needed for effective wavefront compensation for NASA's future ultra-large space telescopes is an optical quality, large-stroke, continuous-membrane deformable mirror (DM) with high actuator density over large areas. DMs with mirror surface quality of <10 nm can be fabricated using the membrane transfer technique demonstrated by our group [1]. Other desirable characteristics of DMs include mirror actuation of >2 μ m at <50V (<1 μ W per pixel), with a bandwidth of > 1kHz, and influence function of <30%. Micromachined DMs have been previously reported, however they needed high-voltage operation due to electrostatic

operation (100-700V) [2-6], small stroke (<2 μ m) [2-4, 6], marginal surface quality [2,4], or high influence function (crosstalk) [3, 4]. Another type of actuators being widely used in DMs are piezoelectric actuators. Many commercial DMs use stacked PZT requiring high voltage operation (~1000V). PZT unimorph-based actuator has a potential to produce a large stroke at relatively low voltage. However, only few detailed studies have conducted on this type of actuator [8]. In this paper, we present a development of thin-film piezoelectric actuator, based on unimorph design in view of their application in DMs.

PZT UNIMORPH ACTUATOR

We have modeled, fabricated and characterized a series of PZT unimorph membrane actuators with various membrane designs in order to optimize the DM actuator geometry. Fig. 1 contains (a) a photograph of fabricated actuators of various types and (b) a schematic illustration of the actuator structure. Electrode designs have been tested. The designs include: full circles, concentric rings, spirals, and segmented electrodes.

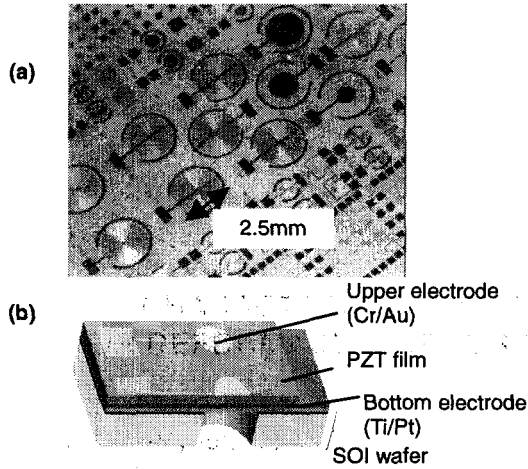


Figure 1. (a) A photograph of PZT actuator array (b) Schematic diagram showing the structure of a PZT unimorph actuator (c) Electrode designs

The actuation principle is as follows: An electric field applied perpendicular to the piezoelectric layer plane induces contraction in the lateral direction, producing a large out-of-plane deflection of the membrane because of its unimorph geometry. Compared to piezoelectric stacks that are widely used in commercial DMs, this actuation mechanism requires far less voltage and power to produce same amount of deflection. We have discovered that there are two regimes of unimorph membrane actuators depending on the PZT film / silicon membrane thickness ratio. For thin silicon membranes (less than or equal to the PZT layer thickness), concentric rings and spiral electrode designs produced more deflection than full circle electrodes, implying that the stress in the electrode film reduces the amount of deflection significantly. For actuators with thick silicon membranes (greater than twice the PZT thickness), full circle electrodes produced more deflection than the other electrode designs. Since actuators with thick Si membranes showed more promise for DM applications because of the higher deflection and ease of handling during fabrication, we focused our efforts in optimizing the full circle actuator design for thick Si membranes.

MODELING FOR PZT UNIMORPH ACTUATOR

In order to optimize the geometry of the unimorph actuator structure, a mathematical model was developed for circular diaphragm with plain circular electrode using an energy minimization method. This modeling was developed based on studies conducted by Muralt *et al.* [8]. First, the following set of functions derived from the thin plate theory are selected as test function for the deflection profile of membrane [9].

$$w(r) = \begin{cases} \lambda \left(\frac{c_1}{4} r^2 + c_2 \ln \frac{r}{a} + c_3 \right) & 0 < r < \beta a \\ \lambda \left(\frac{d_1}{4} r^2 + d_2 \ln \frac{r}{a} + d_3 \right) & \beta a < r < a \end{cases} \quad (1)$$

where r is distance from the center of circle, a is the radius of the membrane, βa is the radius of circular electrode and λ is the Lagrange multiplier. Six unknown coefficients are simultaneously solved by applying boundary conditions at $r=0$, $r=\beta a$, and for clamping at $r=a$. We also define $F(r)$ as $w(r)=\lambda F(r)$ for our convenience. The energy consists of three parts: U_{el} is the elastic energy of the diaphragm under deflection, U_M is the potential energy due to bending moment of piezoelectric film, and U_s is the stretching energy due to the tensile film stresses. These energy terms are given by [8]

$$U_{el} = \frac{1}{2} D \lambda^2 \int_0^a 2\pi r \left[\left(\frac{d^2 F}{dr^2} + \frac{1}{r} \left(\frac{dF}{dr} \right) \right)^2 - 2(1-\nu) \frac{1}{r} \frac{dF}{dr} \frac{d^2 F}{dr^2} \right] dr \quad (2)$$

$$U_s = \frac{1}{2} S \lambda^2 \int_0^a 2\pi r \left(\frac{dF}{dr} \right)^2 dr$$

$$U_M = \frac{1}{2} M \lambda \int_0^{\beta a} 2\pi r \left(\frac{d^2 F}{dr^2} + \frac{1}{r} \frac{dF}{dr} \right) dr$$

D is the flexural rigidity of the circular membrane given by

$$D = \frac{Yh^3}{12(1-\nu^2)} \quad (3)$$

where Y is the Young's modulus, h is the thickness of the membrane and ν is the Poisson's ratio. S is the stretching force per unit length, given by

$$S = S_p + S_f = \beta \sigma_p t_p + \sum \sigma_i \cdot t_i \quad (4)$$

where σ_p is the PZT stress generated in lateral direction, t_p is the thickness of the PZT film, and σ_i is the stress in the i th film of thickness t_i . The factor β originates from the fact that the circumference of the electrode has only β times that of the diaphragm. The bending moment M is obtained as

$$M = \sigma_p t_p \frac{h_{eff}}{2} \quad (5)$$

where $h_{eff}/2$ is the effective distance between the center of the PZT film and the neutral plane of the diaphragm. The total energy of the diaphragm under deflection is therefore

$$U_{tot} = U_{el} + U_s + U_M \quad (6)$$

$$= \frac{1}{2} D \lambda^2 a^2 N_{el}(1, \beta) + \frac{1}{2} S \lambda^2 a^4 N_s(1, \beta) + \frac{1}{2} M \lambda a^2 N_M(1, \beta)$$

where $N_{el}(1, \beta)$ are integrations in equations (2) evaluated at $a=1$. The energy minimization condition, $\partial U_{tot} / \partial \lambda = 0$, yields

$$\lambda_{min} = - \frac{\frac{1}{2} N_M(1, \beta) M}{N_{el}(1, \beta) D + N_s(1, \beta) a^2 S} \quad (7)$$

Hence, the center deflection of the diaphragm is obtained as

$$w(0) = \lambda_{\min} F(0) = 2 \ln 2 \cdot a^2 \lambda_{\min} \quad (8)$$

According to this model, a maximum deflection occurs at an intermediate diaphragm thickness (Fig. 2). It depends on piezoelectric film thickness, piezoelectric stress coefficient (e_{31}) and residual stresses. For this calculation we used $t_p=2\mu\text{m}$, $e_{31}=-6\text{C/m}^2$, and film stress parameters independently obtained from FSM optical stress measurements.

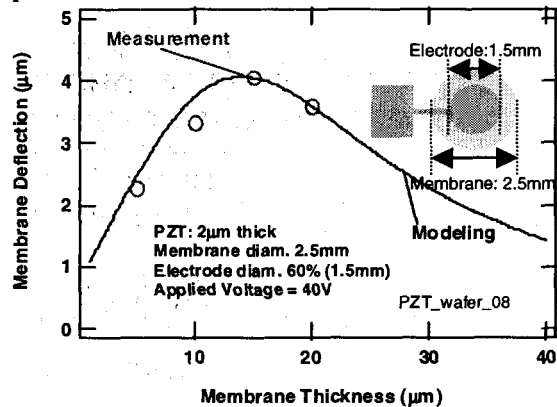


Figure 2. Dependence of deflection on silicon membrane thickness. The data points represent an average of 10 separate measurements on 2 different pixels within a typical array.

EXPERIMENTAL

Lead Zirconate Titanate film preparation

For this study, thick ($>1 \mu\text{m}$) PZT films were prepared using a chemical solution deposition process. The complete film production sequence is shown in Fig. 3. The procedure used was a modification of that first introduced by Budd, *et al.* [10] for processing of PZT films $<2.5 \mu\text{m}$ thick.

Initially, lead acetate trihydrate was added to 2-methoxyethanol (2-MOE) in a rotary evaporator flask under Ar. To facilitate dissolution, the flask was lowered into an oil bath heated to 70°C on a hot plate and the temperature of the bath was gradually increased to 120°C . The solution was then dehydrated under vacuum until a semidry powder remained. A mixture of zirconium *n*-propoxide and titanium iso-propoxide in 2-MOE at room temperature was added and the entire solution was refluxed for 2 hours under Ar at 120°C . After refluxing, the solution was vacuum distilled and 2-MOE was added until the desired solution molarity was achieved. Following modification with both acetylacetone (20 vol%) and acetic acid (5 vol%), the solution was 0.70M with 20mol% Pb in excess of stoichiometry to compensate for high Pb volatility [11].

The substrates used in this study were commercially manufactured Pt(111)/Ti/SiO₂/Si wafers (Nova Electronic Materials, Inc., Richardson, TX) for electrical characterization and platinum coated SOI wafers for device fabrication. Substrates were pre-annealed at 500°C for 60 s. Solutions were dispensed through a syringe with a $0.1\mu\text{m}$ Whatman filter and

the substrate was spun at 1500 rpm for 30s using a photoresist spinner. Two pyrolysis steps, each 60s in duration, were performed using a hot plate at 350 and 500°C , respectively. During the second treatment, a 1-mm-thick aluminum plate was positioned parallel to and about 3.5 mm above the film surface to enhance heating. A crystallization anneal was performed for each layer in a Heatpulse rapid thermal processing unit at 700°C for 60s. Each sequence produced a layer approximately $0.20\mu\text{m}$ in thickness and the sequence was repeated to obtain the desired film thickness.

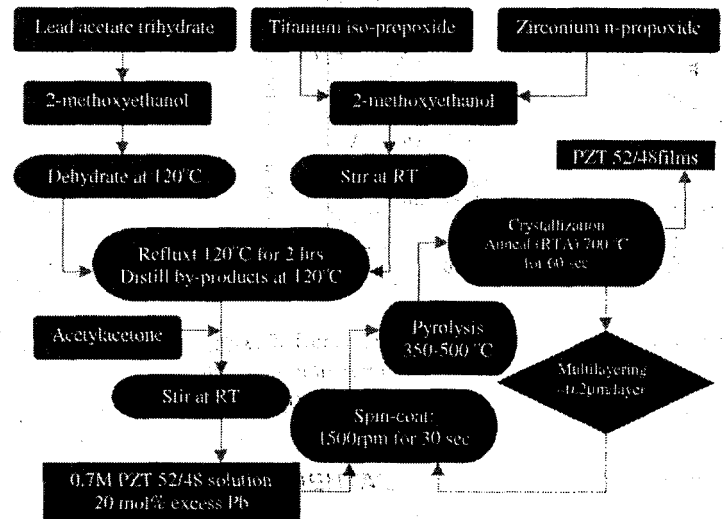


Figure 3. Flowchart of the sol-gel process for PZT films

Film Characterization Methods

Orientation and crystal structure of the PZT films were determined using a Scintag x-ray diffractometer. Ni-filtered Cu $K\alpha$ radiation was used and x-ray diffraction data were collected between 20° and 65° . Microstructural features of the films were examined using a scanning electron microscope.

To enable electrical characterization, Pt/PZT/Pt capacitors were fabricated. For characterization purposes, platinum top electrodes were deposited using a sputter coater through a shadow mask at a base pressure of 0.05–0.1 mbar. Electrodes were circular with a diameter of 0.41 mm and a thickness of approximately 1500\AA . Following deposition, a 5 min hot plate anneal at 500°C was used to improve the quality of the film/top electrode interface. To expose the bottom electrode, a two-step wet etching process for PZT thick films was used [12].

The film thickness was measured using an Alpha-Step surface profilometer. Measurements of capacitance and dielectric loss tangent of the PZT films were performed using an impedance analyzer at 100 kHz and an oscillation voltage of 30 mV. Polarization-electric field hysteresis behavior of the PZT films was measured using an RT66A standardized ferroelectric test system in the virtual ground testing mode.

PZT Film Characterization Results and Discussion

Fig. 4 shows the SEM micrographs of (a) whole thickness of the cross-section, and part of the cross-section of a 6 μm PZT film. As seen in the cross-sectional micrographs, a clear boundary is visible between each crystallized layer and layers appear to be one grain thick. Because each layer was crystallized separately in the rapid thermal annealing, it is likely that the top surface of each layer provided nucleation sites for the layer above it. The grain size is relatively uniform in horizontal and it is about 150nm. Some grains are double or treble size of one layer thickness. This should be due to layer-by-layer homoepitaxy growth within a single grain.

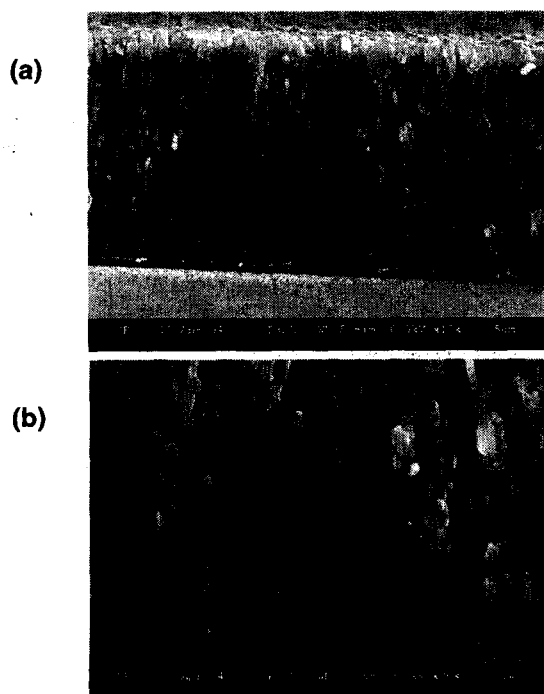


Figure 4. SEM micrographs of (a) whole thickness, and (b) part, of cross-section of a 6 μm PZT film

XRD measurements showed that the films were phase-pure perovskite (i.e., no pyrochlore phase was identified), and had a gradual change in the preferred oriented with increasing film thickness (Fig. 5). When the film thickness was small ($<2\mu\text{m}$), the PZT films had (111) preferred orientation on (111) oriented platinum coated substrates, indicating nucleation from the bottom electrode. With increasing film thickness, the films became more and more randomly oriented as the influence of the Pt/PZT interface was reduced [13].

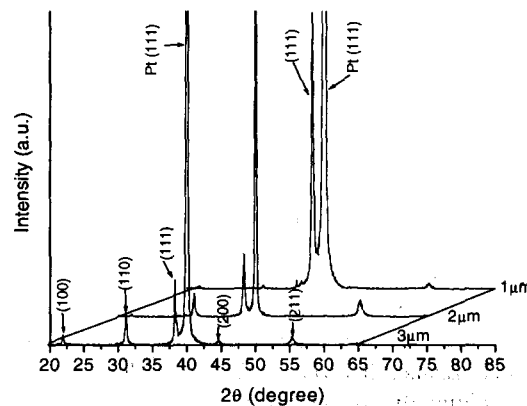


Figure 5. XRD patterns for PZT films with different thickness.

Fig. 7 shows a Polarization-Electric field hysteresis loop of a 1 μm PZT film. The polarization versus applied electric field loop shows a good square shape. Remanent polarization (P_r) and coercive field (E_c) values extracted from the P-E hysteresis loop are 36 $\mu\text{C}/\text{cm}^2$ and 51 kV/cm , respectively. This indicated that the PZT film shows good ferroelectric properties

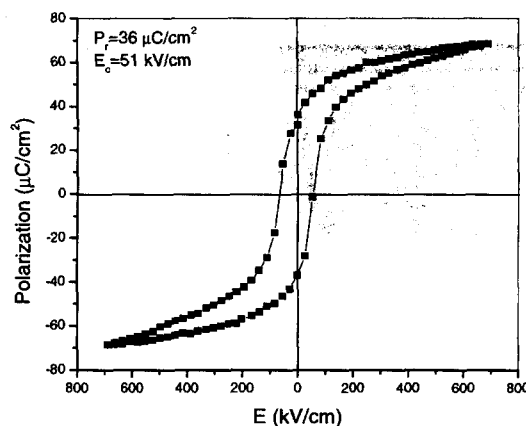


Figure 6. Polarization-Electric field hysteresis loop for 1 μm PZT film.

Relative permittivity was calculated for the capacitance that was measured with HP4192 LF impedance analyzer at 100 kHz and an oscillation voltage of 30 mV. Values of the relative permittivity and tangent loss for a 1 μm PZT film are about 1043 and 2.5% at room temperature, respectively.

Unimorph Actuator Fabrication

PZT coated SOI wafers were further processed. Cr 200 \AA /Au 1500 \AA were evaporated onto the PZT layer, and patterned to form top electrodes and contact pads. A two-step wet etching process for PZT thick films was used to expose the bottom electrode [12]. Finally backside cavities were formed by deep reactive ion etching until buried oxide was exposed.

After the buried oxide was removed in BOE, further reactive ion etching was performed to thin down the silicon membrane if necessary. Kapton tapes were used to cover some areas of the wafer to selectively etch the cavities, thus enabling us to have different silicon membrane thickness from a single wafer.

Interferometer Measurements

A WYKO RST Plus Optical Profiler has been used to analyze the deflections of the membranes. Fig. 7 shows a surface deformation profile of the unimorph actuator under actuation. For 2.5mm diameter actuators with optimized silicon thickness and electrode diameter, we were typically able to obtain 4-5 μm of deflection at <50V.

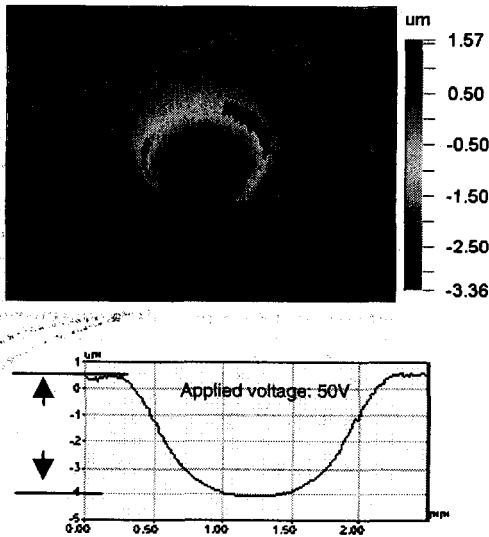


Figure 7. WYKO RST Plus Optical Profiler image of a PZT unimorph actuator under deflection. The thicknesses of PZT/Si layers are 2 μm /15 μm .

Fig. 8 shows a deflection measurements of a unimorph actuator as a function of voltage, showing a typical hysteresis loop of a piezoelectric actuator.

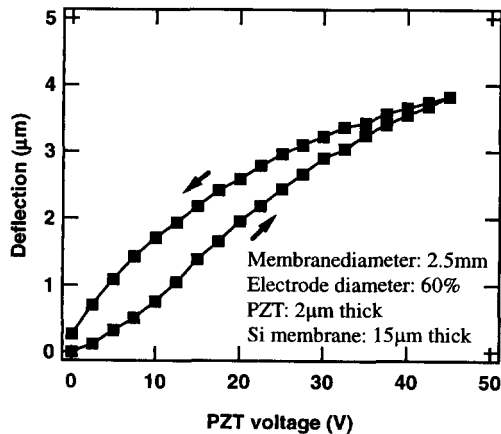


Figure 8. Center deflection of PZT unimorph actuator as a function of applied voltage.

Unimorph actuators with different membrane thickness were fabricated in order to find the optimum thickness (Fig. 1). As predicted by our model, the maximum deflection was obtained at an intermediate membrane thickness (15 μm for PZT of 2 μm thick). Actuators with different diameters of the top electrode were also fabricated and it was found ~60% diameter electrode gives most deflection for the 2 μm PZT/15 μm silicon actuator (Fig. 9).

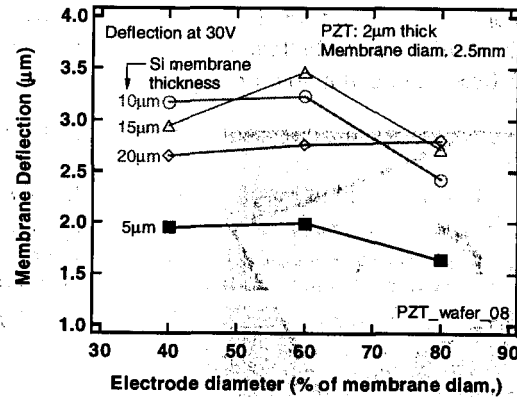


Figure 9. Dependence of membrane deflection on electrode diameter. Optimum electrode diameter is approximately 60% of the membrane diameter.

The frequency response of the actuator was obtained using a laser Doppler vibrometer (Fig. 10). The resonant frequency was observed at 47kHz for the 2.5mm diameter, 2 μm PZT/15 μm Si, 60% electrode actuator, which far exceeds the bandwidth requirement of most DMs (~1kHz).

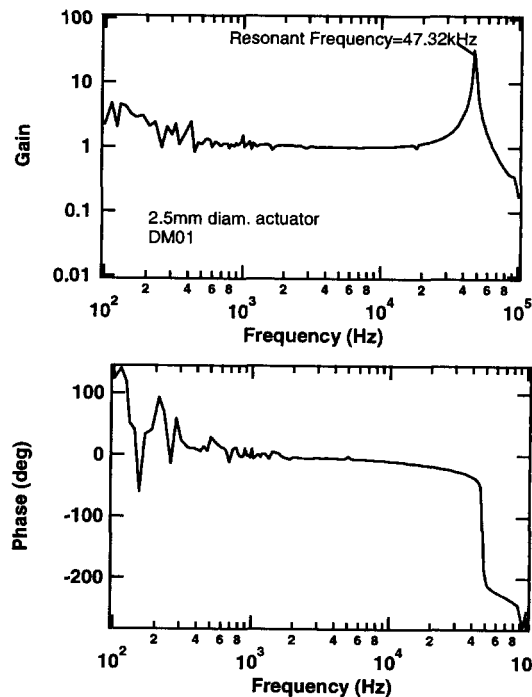


Figure 11. Measured frequency response of PZT unimorph actuator

CONCLUSIONS

PZT unimorph actuators of various electrode designs, silicon membrane thickness, and membrane sizes were fabricated and characterized. A mathematical model based on energy minimization method was developed to assist the optimization of membrane thickness and electrode sizes, and excellent agreement with experiment was obtained. For a 2.5mm diameter actuator with 2 μ m thick PZT and 15 μ m thick silicon membrane, the measured vertical stroke was 5.4 μ m at 50V. The measured resonant frequency of the unimorph actuator was 47kHz, which far exceeds the bandwidth requirement of most DMs (~1kHz). Further work is under way to increase the stroke of actuators, and to incorporate membrane mirror onto an array of actuators.

ACKNOWLEDGEMENTS

The research described in this paper was carried out at the Jet Propulsion Laboratory, California Institute of Technology, under a contract with the National Aeronautics and Space Administration. The research described in this paper was performed under Director's Research and Development Fund at JPL.

REFERENCES

1. E. H. Yang and D. V. Wiberger "A wafer-scale membrane transfer process for the fabrication of optical quality, large continuous membranes," *IEEE/ASME Journal of Microelectromechanical Systems*, 12(6), 804 (2003).
2. T. Bifano *et al.*, "Continuous-Membrane Surface-Micromachined Silicon Deformable Mirror", *Optical Engineering*, 36(5), 1354, (1997); T. Bifano *et al.*, "Micromachined Deformable Mirrors for Adaptive Optics", *SPIE Conf. on High-Resolution Wavefront Control: Methods, Devices, and Applications IV*, Seattle, WA, 7/8-9/2002, SPIE Int. Soc. Opt. Eng.(2002), pp.10-13.
3. J. Mansell *et al.*, "Silicon Deformable Mirrors and CMOS-based Wavefront Sensors," *SPIE International Conference, High-Resolution Wavefront Control*, San Diego, CA, 8/1-2/2000, SPIE Int. Soc. Opt. Eng. (2000), pp.15-25.
4. G. Vdovin, "Optimization-based Operation of Micromachined Deformable Mirrors," *SPIE Conf. on Adaptive Optical System Technology*, Kona, Hawaii, SPIE Int. Soc. Opt. Eng. (1998), pp.902-909.
5. C. Divoux, *et al.*, "A Novel Electrostatic Actuator for Micro Deformable Mirrors: Fabrication and Test", *International Conference on Solid State Sensors, Actuators, and Microsystems*, Boston, MA 6/8-12/03, IEEE(2003), pp.488-491.
6. P. Kurczynski, *et al.*, "Electrostatically actuated membrane mirrors for adaptive optics", *SPIE Conf. on MOEMS and Miniaturized Systems III*, San Jose, CA (2003), pp. 305-313.
7. ref

8. P. Muralt, *et al.*, "Piezoelectric actuation of PZT thin-film diaphragms at static and resonant conditions", *Sensors and Actuators A*, 53, 398 (1996).
9. S. Timoshenko, and S. Woinowsky-Krieger, *Theory of Plates and Shells*, McGraw-Hill, York, 1959.
109. K. D. Budd, S. K. Dey, and D. A. Payne, *Br. Ceram. Proc.* 36, 107 (1985).
11. M. Hendrickson, S. Tao, S. Trolier-McKinstry, B. J. Rod, R. J. Zeto, B. M. Kulwicki, A. Amin, and A. Safari, ISAF '96. Proceedings of the 10th IEEE International Symposium on Applied Ferroelectrics., East Brunswick, NJ, August 18-21, 1996, Vol. 2, p. 683.
12. L.-P. Wang, R. Wolf, Q. Zhou, S. Trolier-McKinstry, and R. J. Davis, "Wet-etch Patterning of Lead Zirconate Titanate (PZT) Thick Films for Microelectromechanical Systems (MEMS) Applications", *Mater. Res. Soc. Symp. Proc.*, Boston, MA, 11/27-28/2000, 657, EE5-39 (2001).
13. R. Kurchania *et al.*, *J. Mater. Res.* 14, 1852 (1999).

ACKNOWLEDGEMENTS

REFERENCES